


Article

Fabrication of Multilayered Two-Dimensional Micelles and Fibers by Controlled Self-Assembly of Rod-Coil Block Copolymers

Rui Qi, Wensheng Qi, Yin Zhang , Baohua Liu, Jian Wang, Hongmei Li, Haimei Yuan and Songzhi Xie *

College of Food and Biological Engineering, Chengdu University, Chengdu 610106, China

* Correspondence: xiesongzhi@cdu.edu.cn

Abstract: Fabricating hierarchical nanomaterials by self-assembly of rod-coil block copolymers attracts great interest. However, the key factors that affect the formation of the hierarchical nanomaterials have not been thoroughly researched. Herein, we have synthesized two diblock copolymers composed of poly(3-hexylthiophene) (P3HT) and polyethylene glycol (PEG). Through a heating, cooling, and aging process, a series of multilayered hierarchical micelles and fibers were prepared in alcoholic solutions. The transition from fibers to hierarchical micelles are strictly influenced by the strength of the π - π stacking interaction, the PEG chain length, and solvent. In isopropanol, the P3HT₂₂-*b*-PEG₄₃ could self-assemble into hierarchical micelles composed of several two-dimensional (2D) laminar layers, driven by the π - π stacking interaction and van der Waals force. The P3HT₂₂-*b*-PEG₄₃ could not self-assemble into well-defined nanostructures in methanol and ethanol, but could self-assemble into fibers in isobutanol. However, the P3HT₂₂-*b*-PEG₁₁₃ with a longer corona block only self-assembled into fibers in four alcoholic solutions, due to the increase in dissolving capacity and steric hindrance. The sizes and the size distributions of the nanostructures both increased with the increase in polymer concentration and the decrease in solvent polarity. This study shows a method to fabricate the hierarchical micelles.

Keywords: hierarchical micelles; rod-coil block polymer; multilayer; two-dimensional; fibers; π - π stacking



Citation: Qi, R.; Qi, W.; Zhang, Y.; Liu, B.; Wang, J.; Li, H.; Yuan, H.; Xie, S. Fabrication of Multilayered Two-Dimensional Micelles and Fibers by Controlled Self-Assembly of Rod-Coil Block Copolymers. *Polymers* **2022**, *14*, 4125. <https://doi.org/10.3390/polym14194125>

Academic Editors: Zhe Sun and Jiating Wen

Received: 30 August 2022

Accepted: 18 September 2022

Published: 2 October 2022

Publisher's Note: MDPI stays neutral with regard to jurisdictional claims in published maps and institutional affiliations.



Copyright: © 2022 by the authors. Licensee MDPI, Basel, Switzerland. This article is an open access article distributed under the terms and conditions of the Creative Commons Attribution (CC BY) license (<https://creativecommons.org/licenses/by/4.0/>).

1. Introduction

Solution self-assembly of block copolymers is a low-cost and effective method to fabricate the defined nanomaterials. By means of adjusting the chemical constituents and the environmental conditions, the block copolymer can self-assemble into various nanostructures, such as spherical micelles [1–3], one-dimensional (1D) micelles [4–8], two-dimensional (2D) micelles [9–11], hierarchical nanostructures [12–15], etc. Recently, fabrication of nanomaterials with hierarchical structures by self-assembly of the block copolymer attracts great interest. Owing to the huge specific surface, hierarchical nanomaterials have great application in many fields, such as templates [16–19], catalysis [20–23], sensors [24–27], etc. To prepare these hierarchical nanomaterials, a variety of methods have been developed [28–30]. Recently, many studies have proven that incorporating additional strong interactions to the assembly systems could favor the fabrication of hierarchical nanomaterials. These strong interactions include hydrogen bonding (H-bonding) [31–33], ionic recognition [34], metal coordination [35–38], crystallinity [39–41], π - π stacking interaction [42,43], etc. For example, Manners et al. [44] prepared a series of hierarchical nanostructures by H-bonding interactions of a homopolymer hydroxyl-functionalized poly(methylvinylsiloxane) (H-bonding donor) and the fibers with a corona block poly(2-vinylpyridine) (H-bonding acceptor). Li et al. [45] synthesized a photo-responsive diblock copolymer poly(ethylene glycol)-*b*-poly(*o*-nitrobenzyl-*L*-glutamate). Upon UV irradiation, the block copolymer could self-assemble into complex micelles induced by the ionic cross-link of Fe³⁺ and carboxylic acid. Due to

the strong π - π stacking interactions, the π -conjugated rod-coil block copolymers show excellent capacity in the fabrication of hierarchical nanomaterials [46,47]. For example, Zhang et al. [48] synthesized an H-shaped block copolymer with bichromophoric perylene diimide as the π -conjugated core. Via the π - π stacking interactions, the H-shaped block copolymer could self-assemble into multilayered rectangles and pyramid-shaped parallelograms in the mixed solvents of chloroform and hexane. However, control over the shapes and sizes of the hierarchical nanomaterials is still challenging. Studying the key factors that affect the transition from the intermediate nanostructures into hierarchical nanomaterials is essential, which would be beneficial to control the morphologies of the nanostructures.

As one of the π -conjugated polymers, poly(3-hexylthiophene) is also widely used to prepare nanomaterials because of its excellent optoelectronic properties [49–52]. In previous studies [53], we prepared a series of regular 2D rectangular micelles by hierarchical self-assembly of poly(3-hexylthiophene) (P3HT)-*b*-polyethylene glycol (PEG) in isopropanol (*i*-PrOH). We proved that the diblock copolymers first self-assembled into fibers and then the fibers were further reorganized to form 2D rectangular micelles, induced by the π - π stacking interaction and the van der Waals force. However, the key factors that affect the transition from the fibers to the 2D rectangular micelles were still obscure. These factors would be beneficial to tailor the sophisticated structures of the hierarchical micelles and the fibers. To find out these factors, herein, we studied the effect of the strength of π - π stacking interaction, the PEG chain length, and solvent on the transition from the fibers to the hierarchical micelles. To achieve this object, the P3HT₂₂ chain, possessing an intermediate strength of π - π stacking interaction, was chosen as the core-forming block in this study. The intermediate strength of π - π stacking interaction would provide an opportunity for us to controllably prepare the hierarchical micelles and fibers. In *i*-PrOH, the transition from fibers to hierarchical micelles was greatly influenced by the PEG chain length. The P3HT₂₂-*b*-PEG₄₃ could self-assemble into multilayered 2D hierarchical micelles in *i*-PrOH. In contrast, the P3HT₂₂-*b*-PEG₁₁₃ could only self-assemble into fibers. As the polymer concentration increased, the sizes of the multilayered 2D hierarchical micelles and fibers all increased. Notably, the P3HT₂₂-*b*-PEG₄₃ could self-assemble into hierarchical micelles composed of vertically stacked 2D lamellar layers and special hierarchical micelles composed of a series of linearly arranged 2D laminar layers, successively, with the increase in polymer concentration in *i*-PrOH. In addition, the self-assembly of the two block copolymers was also influenced by the solvent polarity. The P3HT₂₂-*b*-PEG₄₃ could not self-assemble into well-defined nanostructures in methanol and ethanol, but could self-assemble into fibers in isobutanol. The P3HT₂₂-*b*-PEG₁₁₃ all self-assemble into fibers in four solutions. The length of the fibers increased with the decrease in solvent polarity. This study offers insight into controlling the shapes and sizes of nanostructures.

2. Results and Discussion

2.1. Synthesis and Characterization of the Block Copolymers

The P3HT₂₂-*b*-PEG₄₃ and P3HT₂₂-*b*-PEG₁₁₃ were synthesized according to our previous report [53], as shown in Scheme S1. The two block copolymers were characterized by proton nuclear magnetic resonance spectroscopy (NMR) and gel permeation chromatography (GPC). The chemical shifts of the block copolymers and the molar ratios of the constituents are shown in Figure S1 and Figure S2, which correspond to the theoretical values. The GPC experiments (Figure S3) show that the number-average weights (M_n) of the two block copolymers are 7173 g·mol⁻¹ and 9339 g·mol⁻¹, respectively, which are larger than the M_n (3886 g·mol⁻¹) of the P3HT₂₂ block. The corresponding polydispersity index (PDI) values of the two block polymers are 1.07 and 1.05, respectively, which indicate the narrow distributions. The results of ¹H NMR and GPC demonstrate the successful synthesis of the two block copolymers.

2.2. The Effect of the PEG Chain Length on the Self-Assembly of the Block Copolymer

In previous studies [53], it was found that the sizes and aspect ratios of the 2D rectangular micelles could be controlled by varying the PEG chain length of the block copolymers with a constant long P3HT chain length. However, the shapes of the assemblies did not change with the variation of the PEG chain length, which did not offer adequate support to help us to understand the formation of the 2D micelles. Thus, in order to further understand the effect of the core-forming blocks and corona blocks on the formation of the 2D hierarchical micelles, the P3HT₂₂ chain with an intermediate strength of π - π stacking interaction was selected as a constant core-forming block. In this study, the influence of the PEG chain length on the self-assembly of the block copolymers was first studied in *i*-PrOH at a constant polymer concentration ($c = 0.005 \text{ mg mL}^{-1}$). In solution in *i*-PrOH, the block copolymer P3HT₂₂-*b*-PEG₄₃ self-assembled into 2D hierarchical micelles, which was confirmed by transmission electron microscopy (TEM) (Figure 1a,b). It was found that these 2D hierarchical micelles were composed of several rectangular 2D laminar layers, which was different from the shape of the regular 2D rectangular micelles self-assembled by P3HT₂₂-*b*-PEG₂₂ reported in previous studies [53]. The number-average diagonal length (D_n) of these multilayered hierarchical micelles was 2549 nm, which was slightly larger than the size ($D_n = 2388 \text{ nm}$) of the regular 2D rectangular micelles self-assembled by P3HT₂₂-*b*-PEG₂₂ [53]. This was probably owing to the imperfect stacking of the 2D laminar layers. Figure 2a shows that the diagonal length of these multilayered 2D hierarchical micelles ranged from 800 to 4700 nm, implying a wide distribution. This wide size distribution was also confirmed by the dispersity ($D_w/D_n = 1.09$, D_w —the weight-average diagonal length) of these 2D hierarchical micelles. The size of the rectangular 2D laminar layers included in the multilayered 2D hierarchical micelles was also analyzed. The length of the 2D laminar layers ranged from 800 to 3900 nm (Figure 2b), indicating a wide distribution. The number-average length (L_n) of the 2D laminar layers was 2359 nm, which was slightly larger than the length ($L_n = 2140 \text{ nm}$) of the regular 2D rectangular micelles self-assembled by P3HT₂₂-*b*-PEG₂₂ [53]. This may have contributed to the broad size distribution of the 2D laminar layers. The dispersity ($L_w/L_n = 1.102$, L_w —the weight-average length) and the aspect ratio ($R = 3.234$) of the 2D laminar layers were both larger than the corresponding values of the regular 2D rectangular micelles self-assembled by P3HT₂₂-*b*-PEG₂₂ [53]. As the PEG chain length increased, the variation of the aspect ratio of the 2D nanostructures formed by P3HT₂₂-*b*-PEG_m was in accordance with the corresponding change of the regular 2D rectangular micelles formed by P3HT₄₃-*b*-PEG_m [53]. The standard deviation (σ) of the aspect ratio of the 2D laminar layers was 1.328, implying that the shape of the 2D laminar layers was not uniform. The wide size dispersity and the large standard deviation of the aspect ratio of the 2D laminar layers were probably due to the influences of the intermediate π - π stacking interaction and the variation in PEG chain length.

The multilayered structure of the 2D hierarchical micelles was also confirmed by atomic force microscopy (AFM) (Figure 3a). Figure 3b shows that the heights of the adjacent laminar layers were 3.463 nm, 3.075 nm and 5.616 nm, respectively. The difference in the heights of the adjacent layers indicates that the 2D laminar layers should be composed of a thinner nanostructure. To confirm the formation process of the multilayered 2D hierarchical micelles, we studied the morphologies of the assemblies formed by the P3HT₂₂-*b*-PEG₄₃ when the temperature of the solution decreased to 45 °C. Figure S4a shows the morphologies of the transition structures, which were composed of a series of linearly arranged fibers. This result demonstrates that the P3HT₂₂-*b*-PEG₄₃ first self-assembled into fibers, and then the fibers were further reorganized to form the multilayered 2D hierarchical micelles, as shown Figure 4a,b. The length of the 2D laminar layers should be equal to the contour length of the fibers. The formation process of the multilayered 2D hierarchical micelles is the same as that of the regular 2D rectangular micelles [53].

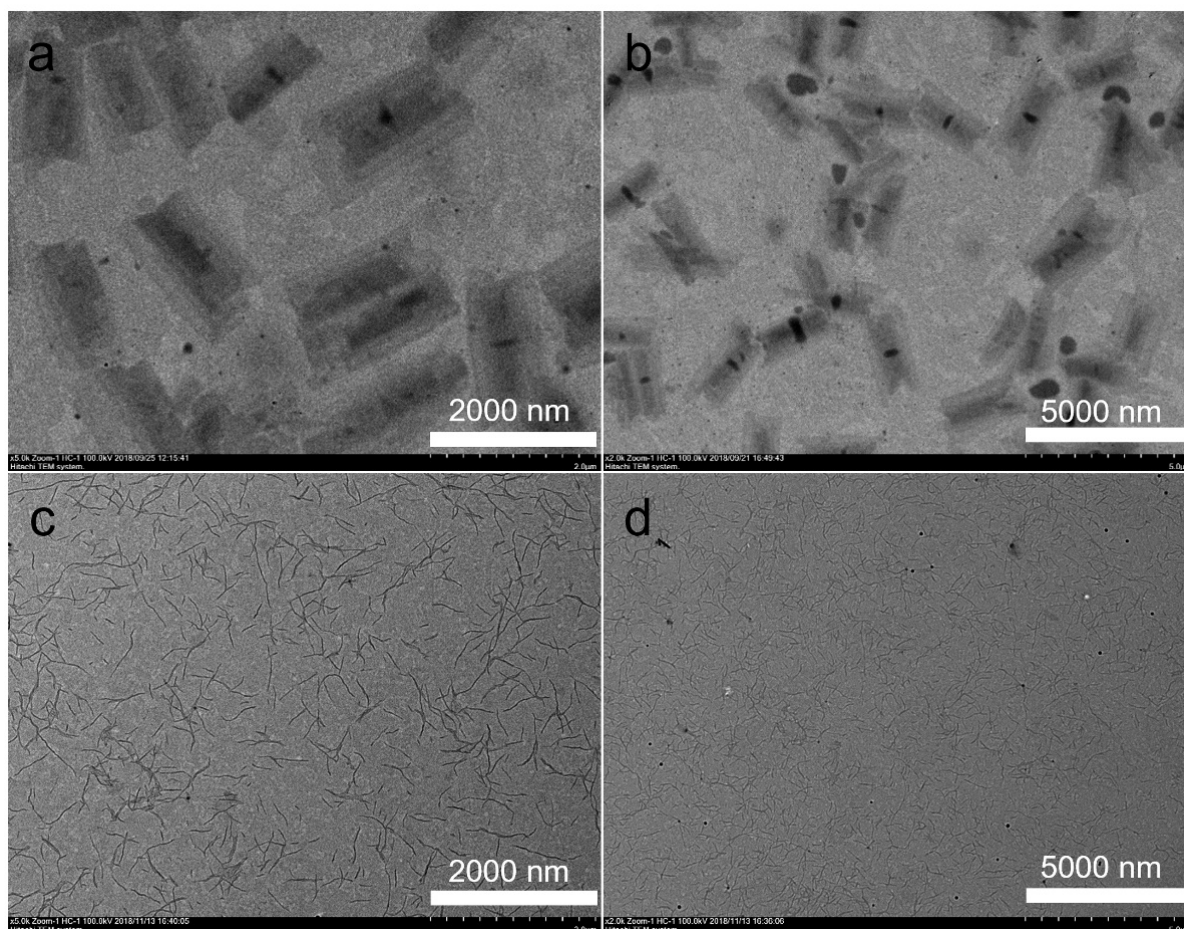


Figure 1. The TEM images of the nanostructures self-assembled by P3HT₂₂-*b*-PEG₄₃ (a,b) and P3HT₂₂-*b*-PEG₁₁₃ (c,d) in *i*-PrOH with the polymer concentration at $c = 0.005 \text{ mg}\cdot\text{mL}^{-1}$.

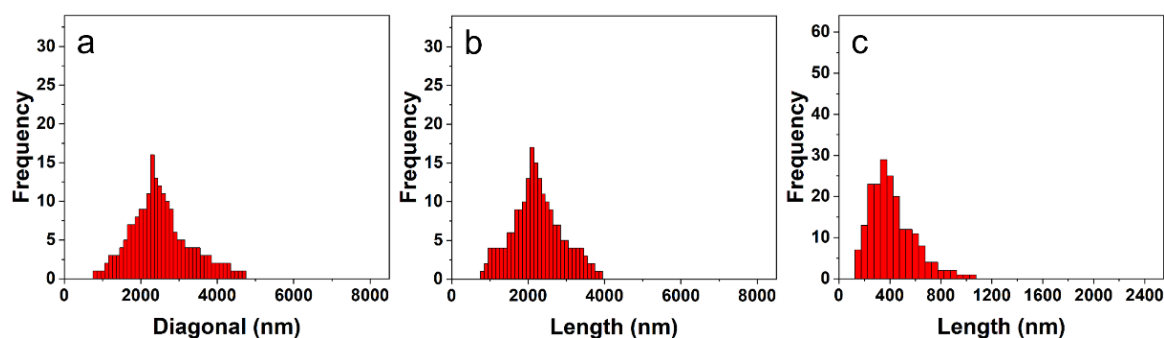


Figure 2. The size distributions of the nanostructures self-assembled by P3HT₂₂-*b*-PEG₄₃ (a,b) and P3HT₂₂-*b*-PEG₁₁₃ (c) in *i*-PrOH with the polymer concentration at $c = 0.005 \text{ mg}\cdot\text{mL}^{-1}$. (a) The diagonal length distribution of the multilayered hierarchical micelles. (b) The length distribution of the 2D laminar layers included in multilayered hierarchical micelles. (c) The contour length of the fibers.

In the *i*-PrOH solution of the P3HT₂₂-*b*-PEG₁₁₃, there were no 2D micelles. The block copolymer all self-assembled into fibers (Figure 1c,d). The number-average contour length (L_n) of these fibers was 440 nm, which was obviously smaller than the length of the 2D laminar layers included in the 2D hierarchical micelles formed by P3HT₂₂-*b*-PEG₄₃. Figure 2c shows that the contour length of these fibers ranged from 150 to 1050 nm, indicating a broad distribution. The dispersity ($L_w/L_n = 1.172$) of the fibers further

confirmed the broad distribution. The AFM result (Figure 3c,d) shows that the height of the fibers was 2.946 nm. The width of the fibers was calculated to be 11.0 nm from the TEM and AFM results. According to the estimation of the sizes of the P3HT₂₂ chain (as shown in Figure S5), the height of the fibers is slightly less than twice the length of side alkyl chain of P3HT, and the width of the fibers is slightly larger than the length of the P3HT₂₂ chain. This result means that the fibers should be composed of two laminar layers of the P3HT₂₂ chain, as shown in Figure S6.

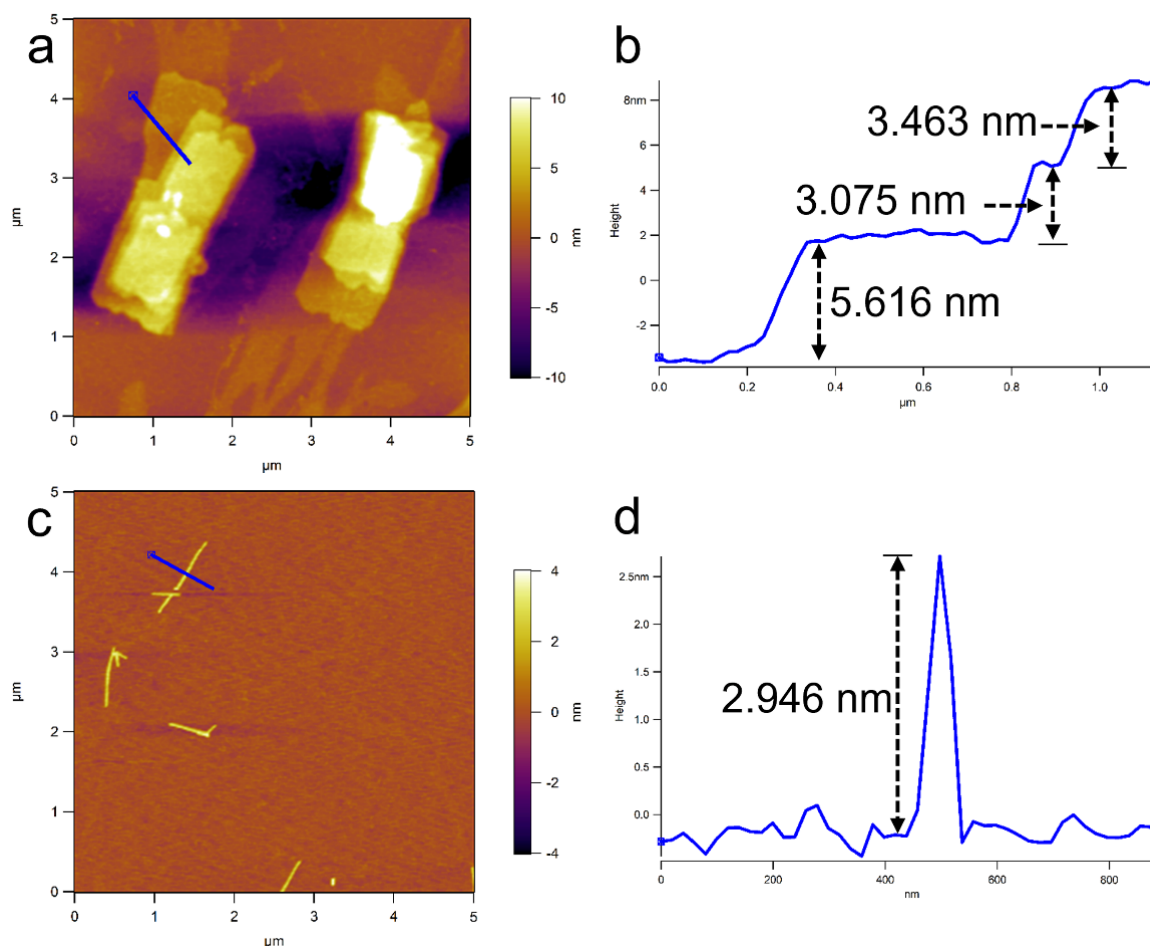


Figure 3. AFM images of the nanostructures self-assembled by P3HT₂₂-*b*-PEG₄₃ (a,b) and P3HT₂₂-*b*-PEG₁₁₃ (c,d) in *i*-PrOH with the polymer concentration at $c = 0.005 \text{ mg} \cdot \text{mL}^{-1}$, the arrows represent the heights of each laminar layer or the single fiber.

The above results prove that the morphologies of the nanostructures were greatly influenced by the variation in PEG chain length, which should be due to the influences of the conjugated P3HT block and PEG block. It is known that the strength of π - π stacking interaction decreases with an decrease in P3HT chain length [54]. Meanwhile, the van der Waals interaction force of the block copolymer with a constant P3HT chain length decreases with an increase in PEG chain length. This is because the dissolving capacity increases with the increase in PEG chain length. In addition, the steric hindrance also increases with the increase in PEG chain length, which favors the formation of the fibers. Thus, the intermediate strength of the π - π stacking interaction and the weaker van der Waals interaction force cannot supply enough force to induce the fibers to form 2D micelles in the solution of the P3HT₂₂-*b*-PEG₁₁₃.

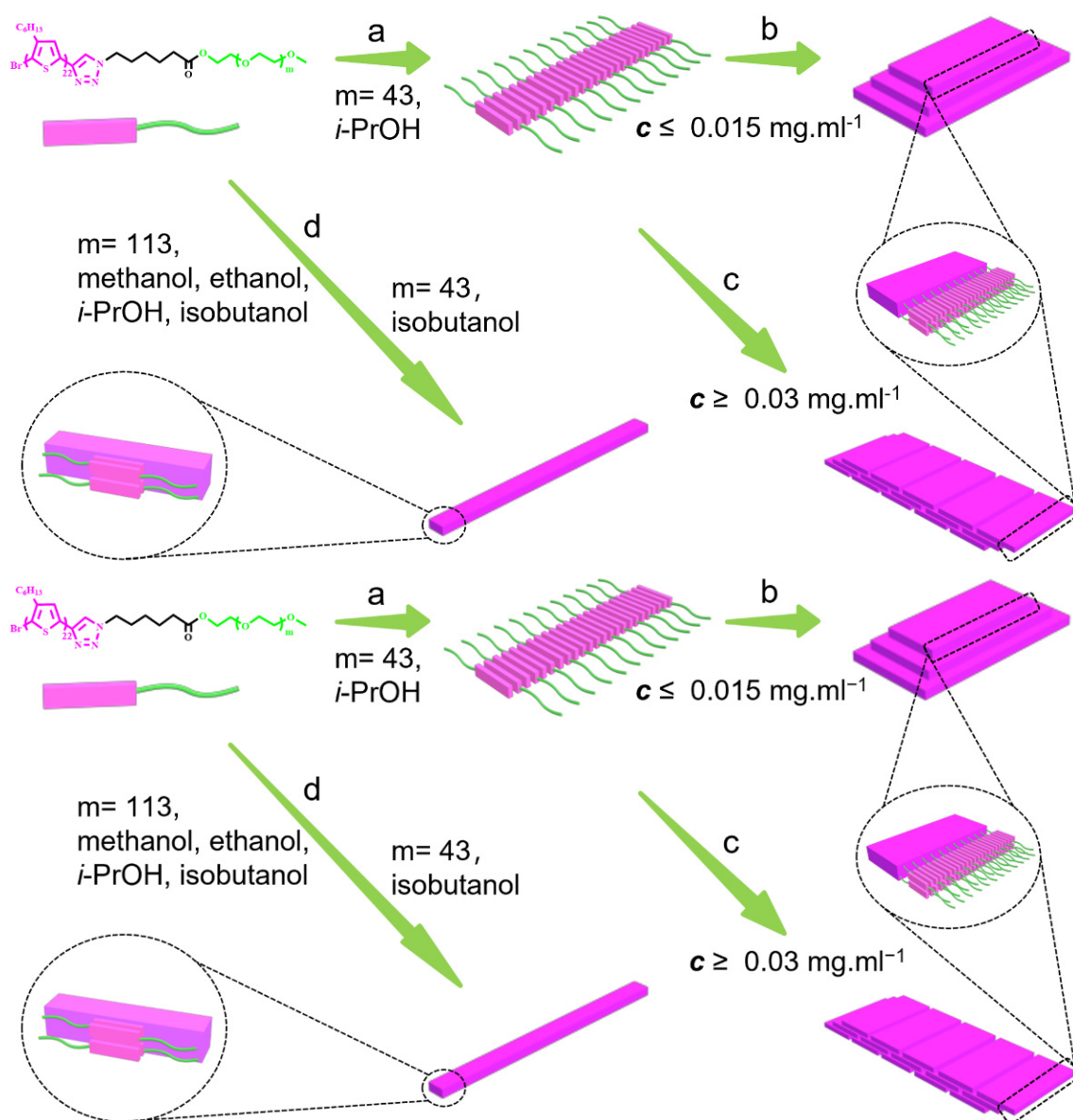


Figure 4. The probable formation processes of the nanostructures self-assembled by $\text{P3HT}_{22}\text{-}b\text{-PEG}_m$, (a) the transition fibers formed by $\text{P3HT}_{22}\text{-}b\text{-PEG}_{43}$ in $i\text{-PrOH}$ during the cooling process, (b) the multilayered hierarchical micelles formed by $\text{P3HT}_{22}\text{-}b\text{-PEG}_{43}$ in $i\text{-PrOH}$ when the polymer concentration is below 0.015 mg.mL^{-1} , (c) the hierarchical micelles with linearly arranged 2D laminae formed by $\text{P3HT}_{22}\text{-}b\text{-PEG}_{43}$ in $i\text{-PrOH}$ when the polymer concentration is above 0.03 mg.mL^{-1} , (d) the fibers formed by $\text{P3HT}_{22}\text{-}b\text{-PEG}_{43}$ in isobutanol, or the fibers formed by $\text{P3HT}_{22}\text{-}b\text{-PEG}_{113}$ in methanol, ethanol, $i\text{-PrOH}$ and isobutanol.

2.3. The Effect of the Polymer Concentration on the Self-Assembly of the Block Copolymer

The influence of the polymer concentration on the self-assembly of the two block copolymers was also investigated. The self-assembly of $\text{P3HT}_{22}\text{-}b\text{-PEG}_{43}$ in $i\text{-PrOH}$ at different polymer concentrations was studied first. In the solution at $c = 0.001 \text{ mg mL}^{-1}$, the block copolymer still self-assembled into 2D hierarchical micelles composed of several 2D laminae layers (Figure 5a and Figure S7a). The D_n of the 2D hierarchical micelles and the L_n of the corresponding 2D laminae layers were 1699 nm and 1570 nm, respectively. The tiny difference in D_n of the 2D hierarchical micelles and in L_n of the corresponding 2D laminae layers indicates that the stacking of the 2D laminae layers was quite good, which could be further confirmed by the statistical size distributions. The statistical diagonal length of the

2D hierarchical micelles ranged from 700 to 3000 nm (Figure 5d). Meanwhile, the statistical length of the 2D laminar layers ranged from 700 to 2900 nm (Figure 5g). The polydispersity of the 2D hierarchical micelles ($D_w/D_n = 1.074$) and the 2D laminar layers ($L_w/L_n = 1.068$) implies good size distributions. The sizes of the 2D hierarchical micelles and their 2D laminar layers obtained in the solution ($c = 0.001 \text{ mg}\cdot\text{mL}^{-1}$) were obviously smaller than the corresponding sizes of the nanostructures obtained in the solution ($c = 0.005 \text{ mg}\cdot\text{mL}^{-1}$). As the polymer concentration increased from 0.005 to $0.015 \text{ mg}\cdot\text{mL}^{-1}$, the sizes of the 2D hierarchical micelles (Figure 5b and Figure S7b,c) and the corresponding 2D laminar layers obviously increased. The D_n of the 2D hierarchical micelles and the L_n of the 2D laminar layers were 2987 nm and 2598 nm, respectively. However, the size distributions of the corresponding nanostructures became broad. Figure 5e shows that the statistical diagonal length of the 2D hierarchical micelles ranged from 900 to 5800 nm. The statistical length of the 2D laminar layers ranged from 600 to 5300 nm, as shown in Figure 5h. The broad distributions were also confirmed by the polydispersity of the 2D hierarchical micelles ($D_w/D_n = 1.173$) and the 2D laminar layers ($L_w/L_n = 1.190$). When the polymer concentration increased from 0.015 to $0.03 \text{ mg}\cdot\text{mL}^{-1}$, amounts of special hierarchical micelles were found (Figure 5c and Figure S7d,e). It was easy to find that these special hierarchical micelles were composed of a series of linearly arranged 2D laminar layers. To further confirm the defined structures of these special hierarchical micelles, we studied the morphologies of the transition structures formed by P3HT₂₂-*b*-PEG₄₃ when the temperature of the solution ($c = 0.03 \text{ mg}\cdot\text{mL}^{-1}$) decreased to 45 °C. Figure S4b shows that the transition structures were composed of a series of linearly arranged fibers. These fibers arranged in a direction that was perpendicular to the length of the fibers. This result further proves that the special hierarchical micelles were formed by the reorganization of the fibers. The length of the linearly arranged 2D laminar layers should be equal to the length of the intermediate fibers. The probable formation process of these special hierarchical micelles is shown in Figure 4c. The D_n of the special hierarchical micelles was 4642 nm, which was observably larger than the D_n of the hierarchical micelles obtained in solutions with lower polymer concentration. This was due to the linear arrangement of the 2D laminar layers included in the special hierarchical micelles. The size distribution of the special hierarchical micelles was very broad, which could be confirmed by the dispersity ($D_w/D_n = 1.211$) and the statistical diagonal length. Figure 5f shows that the statistical diagonal length of the special hierarchical micelles ranged from 1400 to 9300 nm. The L_n of these linearly arranged 2D laminar layers was 2155 nm, which was slightly smaller than the L_n of the 2D laminar layers included in the hierarchical micelles obtained in the solution ($c = 0.015 \text{ mg}\cdot\text{mL}^{-1}$). This should contribute to the broad length distribution ($L_w/L_n = 1.203$) of the 2D laminar layers. Figure 5i shows that the statistical length of the 2D laminar layers ranged from 800 to 5100 nm, further implying a broad distribution. When the polymer concentration was above $0.05 \text{ mg}\cdot\text{mL}^{-1}$, the hierarchical micelles composed of a series of linearly arranged 2D laminar layers could still be found (Figure S7f). The sizes of these hierarchical micelles and the 2D laminar layers were very large and irregular, so they were difficult to measure. The increase in the sizes of the multilayered hierarchical micelles and the corresponding 2D laminar layers with the increase in polymer concentration is shown in Table 1. Table 1 shows that the aspect ratio (R) and the corresponding standard deviation (σ) of the 2D laminar layers increased with an increase in polymer concentration.

In solution in *i*-PrOH, the shapes of the nanostructures formed by the P3HT₂₂-*b*-PEG₁₁₃ were not influenced by the variation in polymer concentration. The diblock copolymer P3HT₂₂-*b*-PEG₁₁₃ all self-assembled into fibers in a wide range of polymer concentrations (Figures 1c and 6a,c,e). However, the sizes of the fibers were distinctly affected by varying the polymer concentration. Figure 6b shows that the contour length of the fibers formed in the solution ($c = 0.001 \text{ mg}\cdot\text{mL}^{-1}$) ranged from 80 to 710 nm. In solution at $c = 0.015 \text{ mg}\cdot\text{mL}^{-1}$, the contour length of the fibers ranged from 90 to 1200 nm (Figure 6d), which was obviously larger than the lengths of the fibers obtained in the solutions ($c = 0.001$ and $0.005 \text{ mg}\cdot\text{mL}^{-1}$). When the polymer concentration increased from 0.015 to $0.03 \text{ mg}\cdot\text{mL}^{-1}$, the contour length

of the fibers continued to increase and ranged from 190 to 2200 nm (Figure 6f). Table 2 shows that the number-average contour length (L_n) of the fibers increased with the increase in polymer concentration. The polydispersity (L_w/L_n) of all the fibers, ranging from 1.170 to 1.350, reveals that all the fibers have broad size distributions and that the size distribution of the fibers became broader with the increase in polymer concentration.

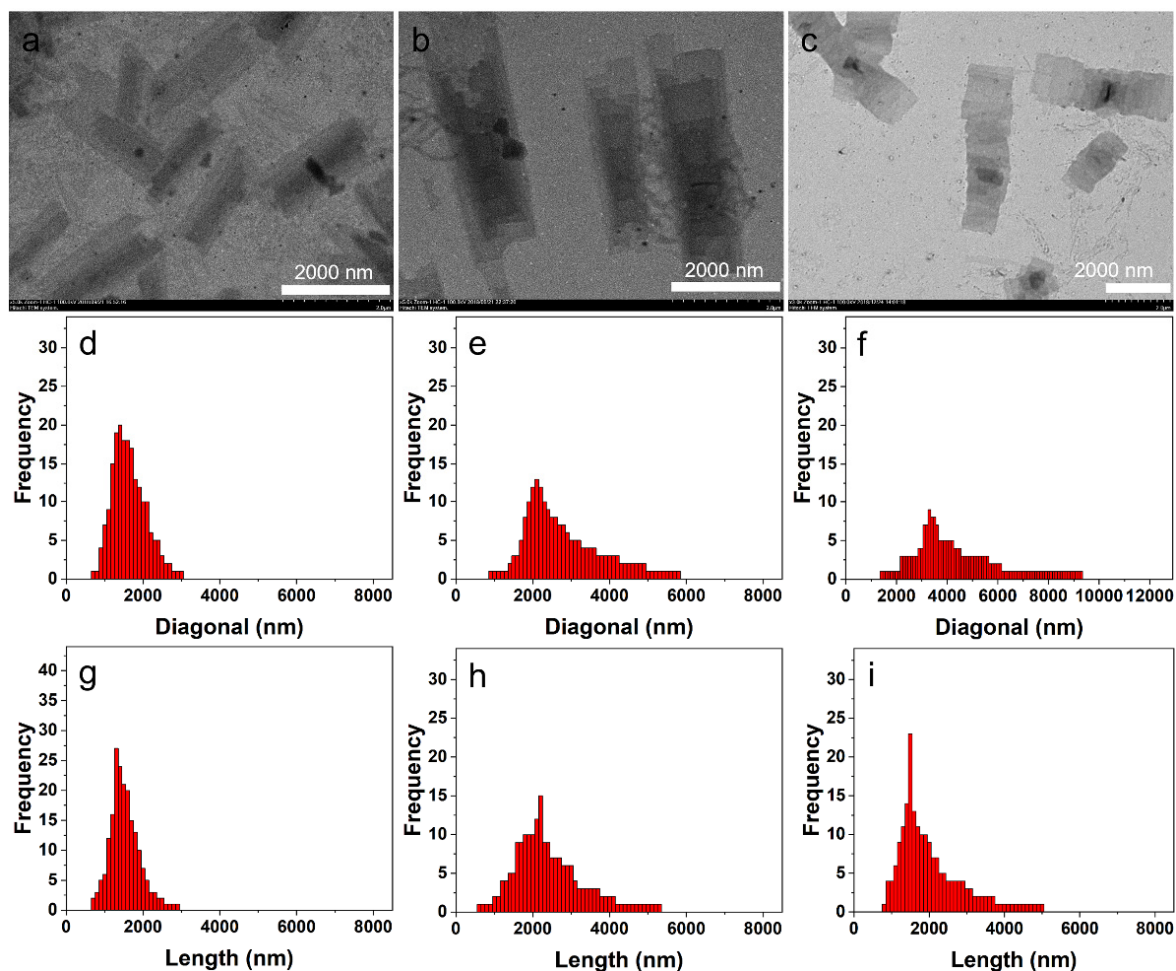


Figure 5. The TEM images and size distributions of the nanostructures self-assembled by P3HT₂₂-*b*-PEG₄₃ in *i*-PrOH with different polymer concentrations. TEM images of the multilayered hierarchical micelles in solutions at $c = 0.001 \text{ mg}\cdot\text{mL}^{-1}$ (a), $c = 0.015 \text{ mg}\cdot\text{mL}^{-1}$ (b), and $c = 0.03 \text{ mg}\cdot\text{mL}^{-1}$ (c). The diagonal length distributions of the multilayered hierarchical micelles in solutions at $c = 0.001 \text{ mg}\cdot\text{mL}^{-1}$ (d), $c = 0.015 \text{ mg}\cdot\text{mL}^{-1}$ (e), and $c = 0.03 \text{ mg}\cdot\text{mL}^{-1}$ (f). The length distributions of the 2D laminar layers included in multilayered hierarchical micelles in solutions at $c = 0.001 \text{ mg}\cdot\text{mL}^{-1}$ (g), $c = 0.015 \text{ mg}\cdot\text{mL}^{-1}$ (h), and $c = 0.03 \text{ mg}\cdot\text{mL}^{-1}$ (i).

Table 1. Summary data of the multilayered hierarchical micelles.

$c \text{ (mg}\cdot\text{mL}^{-1}\text{)}$	$D_w \text{ (nm)}$	$D_n \text{ (nm)}$	D_w/D_n	$L_w \text{ (nm)}$	$L_n \text{ (nm)}$	L_w/L_n	R	σ
0.001	1823	1699	1.074	1677	1570	1.068	2.331	0.947
0.005	2790	2549	1.09	2600	2359	1.102	3.234	1.328
0.015	3503	2987	1.173	3091	2598	1.190	3.440	1.328
0.03	5622	4642	1.211	2593	2155	1.203		

D_w represents the weight-average diagonal length of the multilayered hierarchical micelles; D_n represents the number-average diagonal length of the multilayered hierarchical micelles; L_w represents the weight-average length of the 2D laminar layers included in multilayered hierarchical micelles; L_n represents the number-average length of the 2D laminar layers included in multilayered hierarchical micelles; R represents the aspect ratios of the 2D laminar layers; σ represents the standard deviations of the R .

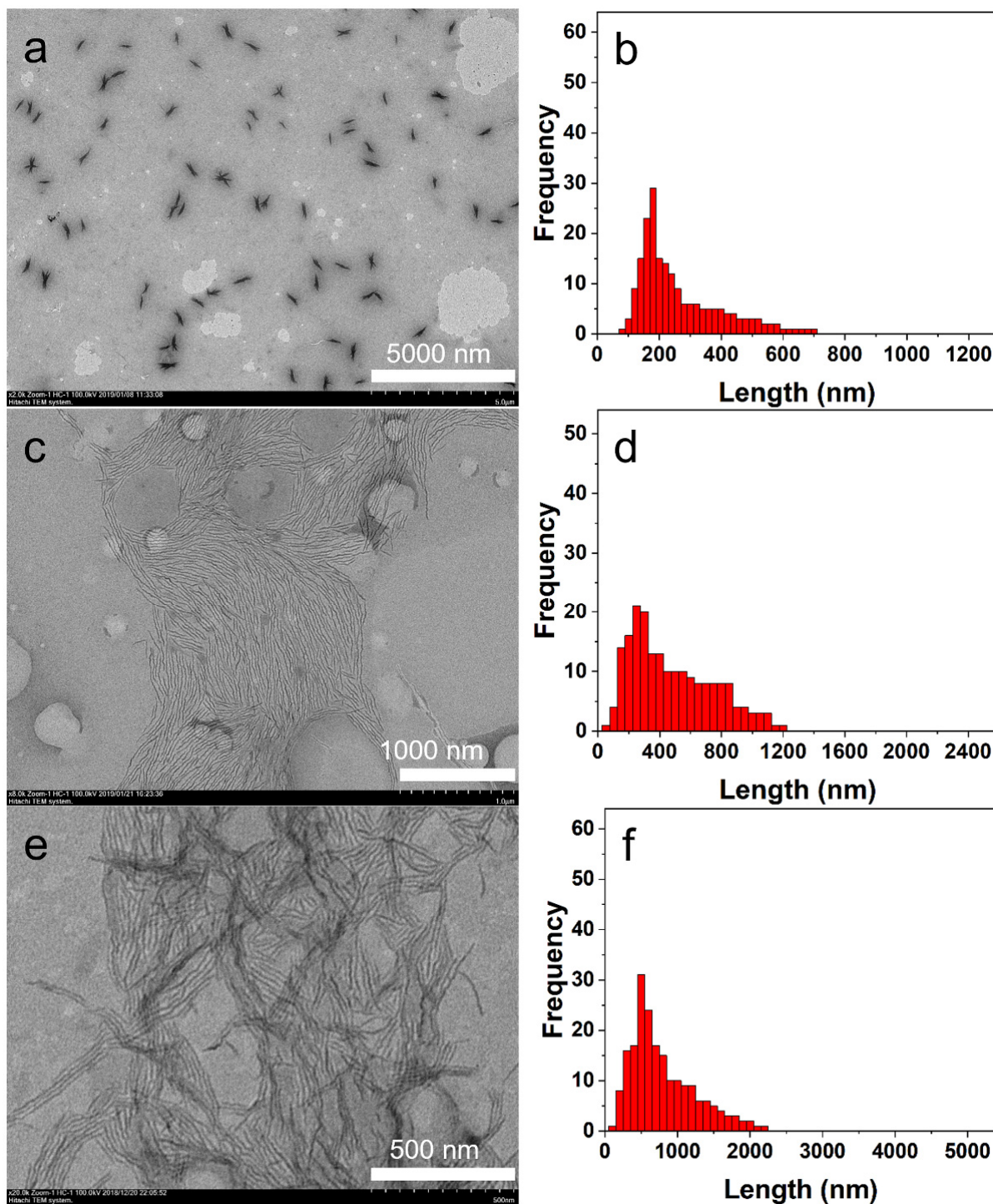


Figure 6. The TEM images and size distributions of the fibers self-assembled by P3HT₂₂-*b*-PEG₁₁₃ in *i*-PrOH with different polymer concentrations. The TEM images of the fibers in solutions at $c = 0.001 \text{ mg}\cdot\text{mL}^{-1}$ (a), $c = 0.015 \text{ mg}\cdot\text{mL}^{-1}$ (c), and $c = 0.03 \text{ mg}\cdot\text{mL}^{-1}$ (e). The length distributions of the fibers in solutions at $c = 0.001 \text{ mg}\cdot\text{mL}^{-1}$ (b), $c = 0.015 \text{ mg}\cdot\text{mL}^{-1}$ (d), and $c = 0.03 \text{ mg}\cdot\text{mL}^{-1}$ (f).

The variation in the sizes of the 2D laminar layers and fibers with the increase in polymer concentration could be explained as follows. As the polymer concentration increases, the Gibbs free energy of the system increases. The formation of nanostructures with larger sizes was more beneficial for reducing the Gibbs free energy of the system. Thus, the lengths of the 2D laminar layers and fibers both increase with an increase in

polymer concentration. Meanwhile, the self-assembly of the block copolymers become more complicated in a higher polymer concentration, resulting in that the aspect ratio (R) and the corresponding standard deviation (σ) of the 2D laminar layers increased with the increase of the polymer concentration.

Table 2. Summary data of the fibers.

Polymers	Solvent	c (mg·mL ⁻¹)	L_n (nm)	L_w (nm)	L_w/L_n
P3HT ₂₂ - <i>b</i> -PEG ₄₃	isobutanol	0.015	1355	2131	1.572
P3HT ₂₂ - <i>b</i> -PEG ₁₁₃	methanol	0.015	95	111	1.170
P3HT ₂₂ - <i>b</i> -PEG ₁₁₃	ethanol	0.015	171	216	1.260
P3HT ₂₂ - <i>b</i> -PEG ₁₁₃	isobutanol	0.015	845	1213	1.436
P3HT ₂₂ - <i>b</i> -PEG ₁₁₃	<i>i</i> -PrOH	0.001	289	368	1.275
P3HT ₂₂ - <i>b</i> -PEG ₁₁₃	<i>i</i> -PrOH	0.005	440	516	1.172
P3HT ₂₂ - <i>b</i> -PEG ₁₁₃	<i>i</i> -PrOH	0.015	513	671	1.306
P3HT ₂₂ - <i>b</i> -PEG ₁₁₃	<i>i</i> -PrOH	0.03	870	1173	1.348

L_w represents the weight-average contour length of the fibers, L_n represents the number-average contour length of the fibers.

2.4. The Effect of the Solvent on the Self-Assembly of the Block Copolymer

The shapes and sizes of the nanostructures can usually be influenced by the solvent because the dissolving capacity, and the interactions of the conjugated blocks could be influenced by the solvent. Thus, the influence of solvents on the self-assembly of the two block copolymers in different solvents was also studied. Owing to their similar molecular structures, methanol, ethanol, and isobutanol were chosen as the additional selective solvents. In fact, the morphologies of the assemblies formed by the P3HT₂₂-*b*-PEG₄₃ were strictly influenced by the solvents. In methanol and ethanol, the diblock copolymer could not self-assemble into well-defined nanostructures (Figure S8a,b). Furthermore, a lot of red precipitates were found in the two solutions during the aging process. In solution in isobutanol ($c = 0.015$ mg·mL⁻¹), the diblock copolymer could only self-assemble into the fibers (Figure S8c) with a number-average contour length (L_n) of 1355 nm. The contour length of these fibers, ranging from 130 to 4000 nm (Figure S8d), implies that these fibers have a broad distribution, which was further confirmed by the dispersity ($L_w/L_n = 1.572$).

In contrast, P3HT₂₂-*b*-PEG₁₁₃ could be dispersed in all three alcohol solutions. The shapes of the nanostructures were not influenced by the variation of the solvent. In methanol, ethanol and isobutanol, the block copolymer all self-assembled into fibers (Figure 7a,c,e). However, the sizes of these fibers were greatly influenced by the variation of the solvent. In solution in methanol ($c = 0.015$ mg·mL⁻¹), the block copolymer self-assembled into very short fibers. Figure 7b shows that contour length of the fibers obtained in methanol, ranging from 30 to 220 nm. In solution in ethanol ($c = 0.015$ mg·mL⁻¹), the contour length of the fibers ranged from 20 to 430 nm (Figure 7d), which was obviously larger than the size of the fibers obtained in methanol. In solution in isobutanol ($c = 0.015$ mg·mL⁻¹), the contour length of the fibers ranged from 140 to 2300 nm. The variation in L_n of these fibers formed in three solutions (shown in Table 2) further confirms the influence of the solvent on the sizes of the fibers. The size distribution (L_w/L_n) of these fibers also increased with a decrease in solvent polarity, as shown in Table 2.

The influence of the solvents on the self-assembly of the two block copolymers could be explained as follows. The dissolving capacity of the block copolymers P3HT₂₂-*b*-PEG _{m} increased with the decrease in solvent polarity and the increase in PEG chain. In methanol and ethanol, the dissolving capacity of the P3HT₂₂-*b*-PEG₄₃ was too poor to self-assemble into well-defined nanostructures. In *i*-PrOH, the dissolving capacity of the P3HT₂₂-*b*-PEG₄₃ increased. The transition structures (fibers) could be reorganized to form multilayered hierarchical micelles, induced by the π - π stacking interaction and van der Waals force. In isobutanol, the dissolving capacity of the P3HT₂₂-*b*-PEG₄₃ greatly increased, leading to a decrease in the interactions of the P3HT₂₂ block. There was not enough force to induce the fibers to form hierarchical micelles. Due to the long PEG chain, the dissolving capacity of

the P3HT₂₂-*b*-PEG₁₁₃ in the four solvents was quite good. The P3HT₂₂-*b*-PEG₁₁₃ could only self-assemble into fibers in all four solvents, due to the increase in dissolving capacity and steric hindrance. The increase in the dissolving capacity of the P3HT₂₂-*b*-PEG_m also leads to an increase in the dispersity of the fibers and a decrease in the length of the fibers.

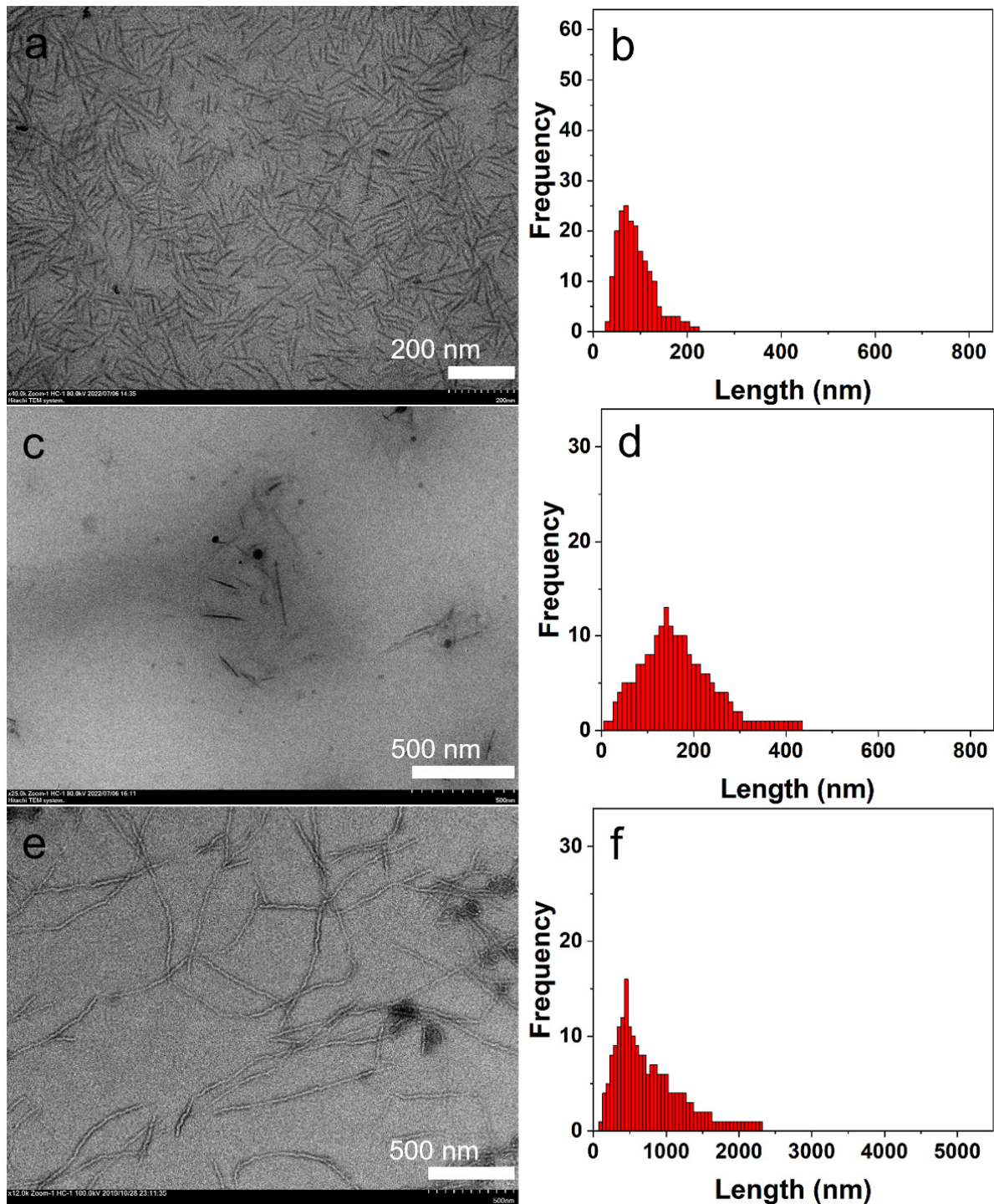


Figure 7. The TEM images and size distributions of the fibers self-assembled by P3HT₂₂-*b*-PEG₁₁₃ in different solvents at $c = 0.015 \text{ mg mL}^{-1}$. The TEM images of the fibers in methanol (a), ethanol (c), and isobutanol (e). The length distributions of the fibers in methanol (b), ethanol (d), and isobutanol (f).

3. Conclusions

In summary, we have prepared a series of multilayered hierarchical micelles self-assembled by P3HT₂₂-*b*-PEG₄₃ and fibers self-assembled by P3HT₂₂-*b*-PEG₁₁₃. The transition from the fibers to the hierarchical micelles has herein been proven to be influenced by the strength of the π - π stacking interaction, the PEG chain length, and solvent. The dissolving capacity and steric hindrance of the block copolymers both increase with an increase in PEG chain length. Meanwhile, the van der Waals force decreases with an increase in PEG chain length. In *i*-PrOH of the P3HT₂₂-*b*-PEG₄₃, the fibers (the transition structures) could be further reorganized to form multi-layered hierarchical micelles, driven by the intermediate strength of the π - π stacking interaction and the van der Waals force. In contrast, the P3HT₂₂-*b*-PEG₁₁₃ with a longer corona block could only self-assemble into fibers in *i*-PrOH, due to the decrease in van der Waals force and the increase in dissolving capacity and steric hindrance. In addition, the shapes and sizes of the nanostructures could be influenced by the polymer concentration and solvent. In *i*-PrOH, the P3HT₂₂-*b*-PEG₄₃ could self-assemble into the hierarchical micelles composed of vertically stacked 2D lamellar layers and the special hierarchical micelles composed of a series of linearly arranged 2D laminar layers, successively, with the increase of the polymer concentration. The P3HT₂₂-*b*-PEG₄₃ could not self-assemble into well-defined nanostructures in methanol and ethanol, but could self-assemble into fibers in isobutanol. The P3HT₂₂-*b*-PEG₁₁₃ could all self-assemble into fibers in methanol, ethanol, and isobutanol. The size and the size distribution of the fibers self-assembled by P3HT₂₂-*b*-PEG₁₁₃ both increase with an increase in polymer concentration and a decrease in solvent polarity. This study will offer insight into controlling the morphologies of nanostructures.

Supplementary Materials: The following supporting information can be downloaded at <https://www.mdpi.com/article/10.3390/polym14194125/s1>. Materials; Synthesis of the di-block copolymer; Preparation of polymer micelles; Polymer Characterization; The statistical sizes of the nanostructures; Scheme S1: Synthesis of P3HT₂₂-*b*-PEG_m; Figure S1: ¹H-NMR spectrum of P3HT₂₂-*b*-PEG₄₃; Figure S2: ¹H-NMR spectrum of P3HT₂₂-*b*-PEG₁₁₃; Figure S3: GPC trace (UV-vis) of P3HT₂₂-*b*-PEG₄₃ and P3HT₂₂-*b*-PEG₁₁₃ in THF; Figure S4: Images of the transition structures self-assembled by P3HT₂₂-*b*-PEG₄₃ when the temperature of the solutions decreased to 45 °C in *i*-PrOH at $c = 0.005 \text{ mg}\cdot\text{mL}^{-1}$ (a) and $c = 0.03 \text{ mg}\cdot\text{mL}^{-1}$ (b) during the cooling processes; Figure S5: The molecular conformation and the corresponding sizes of the P3HT₂₂ chain, calculated with energy minimization (MM2) by ChemBio 3D Ultra; (a) width, (b) length; Figure S6: The probable structures of the fibers self-assembled by P3HT₂₂-*b*-PEG₁₁₃ in *i*-PrOH; Figure S7: The TEM images of the nanostructures self-assembled by P3HT₂₂-*b*-PEG₄₃ in *i*-PrOH with different polymer concentrations of $c = 0.001 \text{ mg}\cdot\text{mL}^{-1}$ (a), $c = 0.015 \text{ mg}\cdot\text{mL}^{-1}$ (b, c), $c = 0.03 \text{ mg}\cdot\text{mL}^{-1}$ (d, e), and $c = 0.05 \text{ mg}\cdot\text{mL}^{-1}$ (f); Figure S8: The TEM images and size distributions of the fibers self-assembled by P3HT₂₂-*b*-PEG₄₃ in different solvents at $c = 0.015 \text{ mg}\cdot\text{mL}^{-1}$; the TEM images of the fibers in methanol (a), ethanol (b), isobutanol (c), and the length distributions of the fibers in isobutanol (d).

Author Contributions: Conceptualization, methodology, writing—original draft preparation, R.Q.; visualization, W.Q.; investigation, Y.Z. and B.L.; software, validation, J.W., H.L. and H.Y.; sources, project administration, writing—review and editing, S.X. All authors have read and agreed to the published version of the manuscript.

Funding: This research was funded by the high-tech talent foundation of Chengdu university (208190244) and Natural Science Foundation of Sichuan Province (2022NSFSC1452).

Data Availability Statement: Not applicable.

Acknowledgments: We acknowledge Tao Fu of Sichuan University for his help with TEM images.

Conflicts of Interest: The authors declare no conflict of interest.

References

1. Klinker, K.; Schafer, O.; Huesmann, D.; Bauer, T.; Capeloa, L.; Braun, L.; Stergiou, N.; Schinnerer, M.; Dirisala, A.; Miyata, K.; et al. Secondary-Structure-Driven Self-Assembly of Reactive Polypept(o)ides: Controlling Size, Shape, and Function of Core Cross-Linked Nanostructures. *Angew. Chem. Int. Ed.* **2017**, *56*, 9608–9613. [[CrossRef](#)] [[PubMed](#)]
2. Li, B.Y.; Li, Y.C.; Lu, Z.Y. The important role of cosolvent in the amphiphilic diblock copolymer self-assembly process. *Polymer* **2019**, *171*, 1–7. [[CrossRef](#)]
3. Qi, R.; Jin, Y.; Cheng, X.F.; Fan, B.Z.; Sun, T.B.; Peng, S.J.; Li, H.P. Crystallization-Driven Self-Assembly of Rod-Coil-Rod Pseudopolyrotaxanes into Spherical Micelles, Nanorods, and Nanorings in Aqueous Solutions. *Macromol. Rapid Commun.* **2015**, *36*, 1402–1408. [[CrossRef](#)] [[PubMed](#)]
4. Jiang, N.S.; Zhang, D.H. Solution Self-Assembly of Coil-Crystalline Diblock Copolypeptoids Bearing Alkyl Side Chains. *Polymers* **2021**, *13*, 3131. [[CrossRef](#)]
5. Qi, R.; Jin, Y. pH- and concentration-controlled self-assembly of spherical micelles with cavity, necklace and cylindrical micelles. *RSC Adv.* **2016**, *6*, 47174–47177. [[CrossRef](#)]
6. Qi, R.; Jin, Y.; Cheng, X.F.; Li, H.P.; Lai, S.Q.; Sun, X.P. Water-Induced Transitions from Ellipsoidal Micelles to Chain-Like Nanostructures Self-Assembled by the Coil-Rod-Coil Block Copolymer Based on Hydrogen-Bonding Urea Groups. *Macromol. Chem. Phys.* **2016**, *217*, 1851–1859. [[CrossRef](#)]
7. Tian, Q.R.; Fei, C.H.; Yin, H.Y.; Feng, Y.J. Stimuli-responsive polymer wormlike micelles. *Prog. Polym. Sci.* **2019**, *89*, 108–132. [[CrossRef](#)]
8. Yin, H.Y.; Feng, Y.J.; Li, P.X.; Douth, J.; Han, Y.X.; Mei, Y.J. Cryogenic viscoelastic surfactant fluids: Fabrication and application in a subzero environment. *J. Colloid Interface Sci.* **2019**, *551*, 89–100. [[CrossRef](#)]
9. Han, L.; Wang, M.J.; Jia, X.M.; Chen, W.; Qian, H.J.; He, F. Uniform two-dimensional square assemblies from conjugated block copolymers driven by pi-pi interactions with controllable sizes. *Nat. Commun.* **2018**, *9*, 865. [[CrossRef](#)]
10. Li, Z.; Zhang, Y.F.; Wu, L.B.; Yu, W.; Wilks, T.R.; Dove, A.P.; Ding, H.M.; O'Reilly, R.K.; Chen, G.S.; Jiang, M. Glyco-Platelets with Controlled Morphologies via Crystallization-Driven Self-Assembly and Their Shape-Dependent Interplay with Macrophages. *ACS Macro Lett.* **2019**, *8*, 596–602. [[CrossRef](#)]
11. Li, Z.Y.; Liu, R.; Mai, B.Y.; Wang, W.J.; Wu, Q.; Liang, G.D.; Gao, H.Y.; Zhu, F.M. Temperature-induced and crystallization-driven self-assembly of polyethylene-b-poly(ethylene oxide) in solution. *Polymer* **2013**, *54*, 1663–1670. [[CrossRef](#)]
12. Kang, L.Y.; Chao, A.; Zhang, M.; Yu, T.Y.; Wang, J.; Wang, Q.; Yu, H.H.; Jiang, N.S.; Zhang, D.H. Modulating the Molecular Geometry and Solution Self-Assembly of Amphiphilic Polypeptoid Block Copolymers by Side Chain Branching Pattern. *J. Am. Chem. Soc.* **2021**, *143*, 5890–5902. [[CrossRef](#)] [[PubMed](#)]
13. Qi, R.; Liu, B.H.; Li, H.M.; Wang, J.; Li, X.H.; Jin, Y.; Xie, S.Z. Formation of ultrathin scarf-like micelles, ultrathin disk-like micelles and spherical micelles by self-assembly of polyurethane diblock copolymers. *J. Mol. Liq.* **2022**, *360*, 119466. [[CrossRef](#)]
14. Sun, S.T.; Xu, S.J.; Zhang, W.D.; Wu, P.Y.; Zhang, W.; Zhu, X.L. Cooperative self-assembly and crystallization into fractal patterns by PNIPAM-based nonlinear multihydrophilic block copolymers under alkaline conditions. *Polym. Chem.* **2013**, *4*, 5800–5809. [[CrossRef](#)]
15. Zheng, T.T.; Feng, H.H.; van den Broek, J.M.; Rahimi, K.; Kuehne, A.J.C.; de Vries, R.; Sprakel, J. Controlling the Hierarchical Assembly of pi-Conjugated Oligoelectrolytes. *Macromol. Rapid Commun.* **2018**, *39*, 1800284 (1-6). [[CrossRef](#)]
16. Li, K.; Yang, J.; Gu, J.L. Hierarchically Porous MOFs Synthesized by Soft-Template Strategies. *Acc. Chem. Res.* **2022**, *55*, 2235–2247. [[CrossRef](#)]
17. Valery, C.; Artzner, F.; Paternostre, M. Peptide nanotubes: Molecular organisations, self-assembly mechanisms and applications. *Soft Matter* **2011**, *7*, 9583–9594. [[CrossRef](#)]
18. Wen, T.; Wang, H.F.; Li, M.C.; Ho, R.M. Homochiral Evolution in Self-Assembled Chiral Polymers and Block Copolymers. *Acc. Chem. Res.* **2017**, *50*, 1011–1021. [[CrossRef](#)]
19. Zollfrank, C.; Cromme, P.; Rauch, M.; Scheel, H.; Kostova, M.H.; Gutbrod, K.; Gruber, S.; Van Opdenbosch, D. Biotemplating of inorganic functional materials from polysaccharides. *Bioinspired Biomimetic Nanobiomater.* **2012**, *1*, 13–25. [[CrossRef](#)]
20. Cameron, J.M.; Guillemot, G.; Galambos, T.; Amin, S.S.; Hampson, E.; Haidaraly, K.M.; Newton, G.N.; Izzet, G. Supramolecular assemblies of organo-functionalised hybrid polyoxometalates: From functional building blocks to hierarchical nanomaterials. *Chem. Soc. Rev.* **2022**, *51*, 293–328. [[CrossRef](#)]
21. Dong, R.H.; Pfeffermann, M.; Liang, H.W.; Zheng, Z.K.; Zhu, X.; Zhang, J.; Feng, X.L. Large-Area, Free-Standing, Two-Dimensional Supramolecular Polymer Single-Layer Sheets for Highly Efficient Electrocatalytic Hydrogen Evolution. *Angew. Chem. Int. Ed.* **2015**, *54*, 12058–12063. [[CrossRef](#)] [[PubMed](#)]
22. Gong, C.C.; Sun, S.W.; Zhang, Y.J.; Sun, L.; Su, Z.Q.; Wu, A.G.; Wei, G. Hierarchical nanomaterials via biomolecular self-assembly and bioinspiration for energy and environmental applications. *Nanoscale* **2019**, *11*, 4147–4182. [[CrossRef](#)]
23. Tian, J.; Zhang, Y.F.; Du, L.L.; He, Y.X.; Jin, X.H.; Pearce, S.; Eloi, J.C.; Harniman, R.L.; Alibhai, D.; Ye, R.Q.; et al. Tailored self-assembled photocatalytic nanofibres for visible-light-driven hydrogen production. *Nat. Chem.* **2020**, *12*, 1150. [[CrossRef](#)] [[PubMed](#)]
24. Datta, S.; Saha, M.L.; Stang, P.J. Hierarchical Assemblies of Supramolecular Coordination Complexes. *Acc. Chem. Res.* **2018**, *51*, 2047–2063. [[CrossRef](#)] [[PubMed](#)]

25. Wang, J.; Eijkel, J.C.T.; Jin, M.L.; Xie, S.T.; Yuan, D.; Zhou, G.F.; van den Berg, A.; Shui, L.L. Microfluidic fabrication of responsive hierarchical microscale particles from macroscale materials and nanoscale particles. *Sens. Actuator B-Chem.* **2017**, *247*, 78–91. [[CrossRef](#)]
26. Zhang, Y.F.; Pearce, S.; Eloi, J.C.; Harniman, R.L.; Tian, J.; Cordoba, C.; Kang, Y.T.; Fukui, T.; Qiu, H.B.; Blackburn, A.; et al. Dendritic Micelles with Controlled Branching and Sensor Applications. *J. Am. Chem. Soc.* **2021**, *143*, 5805–5814. [[CrossRef](#)] [[PubMed](#)]
27. Zhu, G.X.; Liu, Y.J.; Xi, C.Y.; Bao, C.L.; Xu, H.; Shen, X.P.; Zhu, X.L. Polymer guided synthesis of Ni(OH)₂ with hierarchical structure and their application as the precursor for sensing materials. *Crystengcomm* **2013**, *15*, 9189–9195. [[CrossRef](#)]
28. Hils, C.; Manners, I.; Schobel, J.; Schmalz, H. Patchy Micelles with a Crystalline Core: Self-Assembly Concepts, Properties, and Applications. *Polymers* **2021**, *13*, 1481. [[CrossRef](#)]
29. Karayianni, M.; Pispas, S. Block copolymer solution self-assembly: Recent advances, emerging trends, and applications. *J. Polym. Sci.* **2021**, *59*, 1874–1898. [[CrossRef](#)]
30. Milton, M.; Deng, R.; Mann, A.; Wang, C.Y.; Tang, D.N.; Weck, M. Secondary Structure in Nonpeptidic Supramolecular Block Copolymers. *Acc. Chem. Res.* **2021**, *54*, 2397–2408. [[CrossRef](#)]
31. Adhikari, B.; Lin, X.; Yamauchi, M.; Ouchi, H.; Aratsua, K.; Yagai, S. Hydrogen-bonded rosettes comprising pi-conjugated systems as building blocks for functional one-dimensional assemblies. *Chem. Commun.* **2017**, *53*, 9663–9683. [[CrossRef](#)]
32. Liang, J.Q.; Guo, P.P.; Qin, X.J.; Gao, X.H.; Ma, K.; Zhu, X.F.; Jin, X.; Xu, W.W.; Jiang, L.X.; Duan, P.F. Hierarchically Chiral Lattice Self-Assembly Induced Circularly Polarized Luminescence. *ACS Nano* **2020**, *14*, 3190–3198. [[CrossRef](#)]
33. Yagai, S. Supramolecularly Engineered Functional pi-Assemblies Based on Complementary Hydrogen-Bonding Interactions. *Bull. Chem. Soc. Jpn.* **2015**, *88*, 28–58. [[CrossRef](#)]
34. Xu, L.M.; Jiang, L.X.; Drechsler, M.; Sun, Y.; Liu, Z.R.; Huang, J.B.; Tang, B.Z.; Li, Z.B.; Stuart, M.A.C.; Yan, Y. Self-Assembly of Ultralong Polyion Nanoladders Facilitated by Ionic Recognition and Molecular Stiffness. *J. Am. Chem. Soc.* **2014**, *136*, 1942–1947. [[CrossRef](#)] [[PubMed](#)]
35. Jiang, H.; Jelinek, R. Hierarchical Assembly of Polydiacetylene Microtube Biosensors Mediated by Divalent Metal Ions. *ChemPlusChem* **2016**, *81*, 119–124. [[CrossRef](#)]
36. Kartha, K.K.; Allampally, N.K.; Politi, A.T.; Prabhu, D.D.; Ouchi, H.; Albuquerque, R.Q.; Yagai, S.; Fernandez, G. Influence of metal coordination and light irradiation on hierarchical self-assembly processes. *Chem. Sci.* **2019**, *10*, 752–760. [[CrossRef](#)]
37. Lunn, D.J.; Gould, O.E.C.; Whittell, G.R.; Armstrong, D.P.; Mineart, K.P.; Winnik, M.A.; Spontak, R.J.; Pringle, P.G.; Manners, I. Microfibrils and macroscopic films from the coordination-driven hierarchical self-assembly of cylindrical micelles. *Nat. Commun.* **2016**, *7*, 12371. [[CrossRef](#)] [[PubMed](#)]
38. Zhou, X.Q.; Jin, Q.X.; Zhang, L.; Shen, Z.C.; Jiang, L.; Liu, M.H. Self-Assembly of Hierarchical Chiral Nanostructures Based on Metal-Benzimidazole Interactions: Chiral Nanofibers, Nanotubes, and Microtubular Flowers. *Small* **2016**, *12*, 4743–4752. [[CrossRef](#)]
39. He, Y.X.; Eloi, J.C.; Harniman, R.L.; Richardson, R.M.; Whittell, G.R.; Mathers, R.T.; Dove, A.P.; O'Reilly, R.K.; Manners, I. Uniform Biodegradable Fiber-Like Micelles and Block Comicelles via “Living” Crystallization-Driven Self-Assembly of Poly(-lactide) Block Copolymers: The Importance of Reducing Unimer Self-Nucleation via Hydrogen Bond Disruption. *J. Am. Chem. Soc.* **2019**, *141*, 19088–19098. [[CrossRef](#)]
40. Inam, M.; Cambridge, G.; Pitto-Barry, A.; Laker, Z.P.L.; Wilson, N.R.; Mathers, R.T.; Dove, A.P.; O'Reilly, R.K. 1D vs. 2D shape selectivity in the crystallization-driven self-assembly of polylactide block copolymers. *Chem. Sci.* **2017**, *8*, 4223–4230. [[CrossRef](#)] [[PubMed](#)]
41. Song, S.F.; Liu, X.M.; Nikbin, E.; Howe, J.Y.; Yu, Q.; Manners, I.; Winnik, M.A. Uniform 1D Micelles and Patchy & Block Comicelles via Scalable, One-Step Crystallization-Driven Block Copolymer Self-Assembly. *J. Am. Chem. Soc.* **2021**, *143*, 6266–6280.
42. Goel, M.; Narasimha, K.; Jayakannan, M. Helical Self-Assemblies of Segmented Poly(phenylenevinylene)s and Their Hierarchical Donor-Acceptor Complexes. *Macromolecules* **2014**, *47*, 2592–2603. [[CrossRef](#)]
43. Wang, M.T.; Han, L.; Zhu, Y.L.; Qi, R.; Tian, L.L.; He, F. Formation of Hierarchical Architectures with Dimensional and Morphological Control in the Self-Assembly of Conjugated Block Copolymers. *Small Methods* **2020**, *4*, 1900470. [[CrossRef](#)]
44. Li, X.Y.; Gao, Y.; Harniman, R.; Winnik, M.; Manners, I. Hierarchical Assembly of Cylindrical Block Comicelles Mediated by Spatially Confined Hydrogen-Bonding Interactions. *J. Am. Chem. Soc.* **2016**, *138*, 12902–12912. [[CrossRef](#)]
45. Ji, S.F.; Xu, L.L.; Fu, X.H.; Sun, J.; Li, Z.B. Light- and Metal Ion-Induced Self-Assembly and Reassembly Based on Block Copolymers Containing a Photoresponsive Polypeptide Segment. *Macromolecules* **2019**, *52*, 4686–4693. [[CrossRef](#)]
46. Wang, M.J.; Zhu, Y.L.; Han, L.; Qi, R.; He, F. Inky flower-like supermicelles assembled from pi-conjugated block copolymers. *Polym. Chem.* **2020**, *11*, 61–67. [[CrossRef](#)]
47. Yu, Z.; Lu, K.; Wei, Z.X. Self-assembly of conjugated polymers for anisotropic nanostructures. *Sci. China-Chem.* **2012**, *55*, 2283–2291. [[CrossRef](#)]
48. Huang, Y.J.; Yu, F.; Cao, X.; Nie, L.; Zhang, P.F.; Xu, F.G.; Gong, Q.Y.; Zhan, X.J.; Zhao, K.X.; Huang, Y.Z.; et al. Tunable low-dimensional self-assembly of H-shaped bichromophoric peryleneimide Gemini in solution. *Nanoscale* **2020**, *12*, 3058–3067. [[CrossRef](#)]
49. Jo, G.; Jung, J.; Chang, M. Controlled Self-Assembly of Conjugated Polymers via a Solvent Vapor Pre-Treatment for Use in Organic Field-Effect Transistors. *Polymers* **2019**, *11*, 332. [[CrossRef](#)]

50. Persson, N.E.; Chu, P.H.; McBride, M.; Grover, M.; Reichmanis, E. Nucleation, Growth, and Alignment of Poly(3-hexylthiophene) Nanofibers for High-Performance OFETs. *Acc. Chem. Res.* **2017**, *50*, 932–942. [[CrossRef](#)] [[PubMed](#)]
51. Tu, T.H.; Chan, Y.T. Synthesis of Terpyridine End-Modified Polystyrenes through ATRP for Facile Construction of Metallo-Supramolecular P3HT-*b*-PS Diblock Copolymers. *Polymers* **2020**, *12*, 2842. [[CrossRef](#)]
52. Ye, S.; Lotocki, V.; Xu, H.; Seferos, D.S. Group 16 conjugated polymers based on furan, thiophene, selenophene, and tellurophene. *Chem. Soc. Rev.* **2022**, *51*, 6442–6474. [[CrossRef](#)]
53. Qi, R.; Zhu, Y.L.; Han, L.; Wang, M.J.; He, F. Rectangular Platelet Micelles with Controlled Aspect Ratio by Hierarchical Self-Assembly of Poly(3-hexylthiophene)-*b*-poly(ethylene glycol). *Macromolecules* **2020**, *53*, 6555–6565. [[CrossRef](#)]
54. Lee, M.J.; Jeon, H.; Jang, M.; Yang, H. A Physicochemical Approach Toward Extending Conjugation and the Ordering of Solution-Processable Semiconducting Polymers. *ACS Appl. Mater. Interfaces* **2016**, *8*, 4819–4827. [[CrossRef](#)]